Red-green-blue model

David B. Wilson
Microsoft Research, One Microsoft Way, Redmond, Washington 98052, USA
(Received 3 December 2002; published 31 March 2004)

We experimentally study the red-green-blue model, which is a system of loops obtained by superimposing three dimer coverings on offset hexagonal lattices. We find that when the boundary conditions are ''flat,'' the red-green-blue loops are closely related to stochastic Loewner evolution with parameter $\kappa=4$ (SLE_4) and double-dimer loops, which are the loops formed by superimposing two dimer coverings of the Cartesian lattice. But we also find that the red-green-blue loops are more tightly nested than the double-dimer loops. We also investigate the two-dimensional minimum spanning tree, and find that it is not conformally invariant.

DOI: 10.1103/PhysRevE.69.037105 PACS number(s): 05.50.+q, 64.60.Fr, 64.60.Ak

I. INTRODUCTION

We investigate the red-green-blue (RGB) model, which was introduced by Benjamini and Schramm [1]. A RGB configuration is a system of the loops on a region of the triangular lattice, which is obtained by superimposing three perfect matchings (or dimer coverings) on offset hexagonal lattices as shown in Fig. 1. The sites of the triangular lattice may be three-colored so that no two adjacent sites have the same color. If we delete the sites of a given color (say blue), then the sites of the other two colors (red and green) form a hexagonal lattice on which we can construct a random perfect matching (the blue perfect matching). When we superimpose the red, green, and blue perfect matchings, each vertex is matched with one neighboring vertex of each of the other two colors. Since each vertex has degree two, a RGB configuration consists of closed loops, and each loop has an orientation if we follow the edges in the order red to green to blue.

It is worth remarking that the boundary conditions of dimer systems can have a profound impact on the behavior of dimers even far within the interior of a region [2–4]. There are height functions associated with dimer configurations on the Cartesian lattice [5,6] and hexagonal lattice [7] (see also [8,9]). If there is an imbalance between the different colors of vertices along the boundary, then the height along the boundary will be ''tilted,'' and this affects the dimers throughout the region. Consequently, the behavior of the RGB model on regions with tilted boundary conditions could be different from the behavior of the RGB model on the regions that we consider here, where the three color classes along the boundary are balanced (''flat'' boundary conditions).

In an earlier work, Kenyon and the author [10] found experimentally that the fractal dimension of these loops is 3/2. Here we report on additional experiments, where we find that the winding angle variance at a typical point on a loop is $1\times\log D$ where D is the diameter of the loop, and that the system of loops appears to be conformally invariant. These properties suggest that the RGB loops are closely related to stochastic Loewner evolution [11] with parameter $\kappa=4$ (SLE_4), and that the RGB loops belong to the same universality class as the contours of two-dimensional (2D) Fortuin-Kasteleyn (FK) [12] clusters at criticality when $q=4$, and the loops formed in the double-dimer (or ''double-domino'') model [13], which in turn are thought to correspond to the ''contours'' of a Gaussian-free field [13]. However, the system of RGB loops does not have the same limiting behavior as the system of double-dimer loops, because we also find that the RGB loops are more tightly nested than the double-dimer loops.

II. GENERATING RGB CONFIGURATIONS

To generate a RGB configuration of a region, we need to generate dimer coverings of three regions of the hexagonal lattice. There are many ways to generate dimer coverings of the hexagonal lattice, but the fastest of these is based on a generalization of Temperley's bijection [14] between spanning trees and dimers. To generate the perfect matchings on the hexagonal lattice, the corresponding spanning trees are on a directed triangular lattice (see [15] for details), and these spanning trees may be quickly generated using an algorithm based on loop-erased random walk [16]. This generalized-Temperley bijection only works for regions of the hexagonal lattice that have certain special (very flat) boundary conditions, so we can only expect to use it to generate RGB configurations of certain regions. One region where we can use spanning trees to rapidly generate RGB configurations is the equilateral triangle with side length $3L$ (Figs. 1 and 2).

III. WINDINESS OF RGB LOOPS

We recall the definition of the windiness of a loop used in [17]. Consider an ant which travels along the loop; after the ant has just traversed a given edge in the loop, before traversing the next edge it will either turn left 120°, turn right 120°, or not turn at all. If we keep track of the total turning (measured in radians) when the ant travels from point A to point B on the loop, then this is (approximately) the winding angle between points A and B. When the ant travels all the way around the loop, it has turned $\pm 360°$, so to make the winding angle between points A and B independent of the number of times that the ant travels around the loop and the direction of travel, we adjust the total turning (measured in radians) by $2\pi\times$ [number of steps between A and B]/[length of loop]. To define the winding angle at a given point X

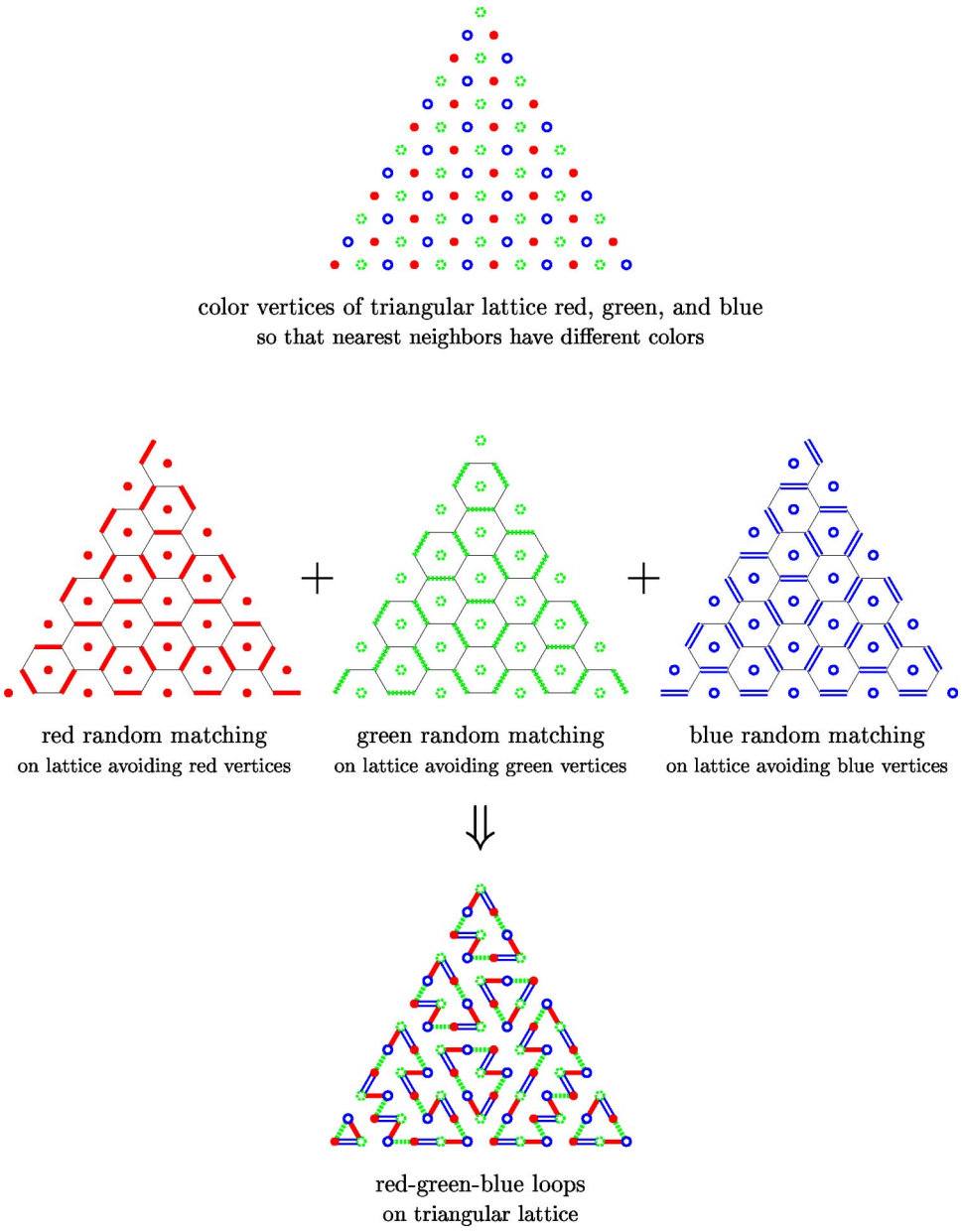

FIG. 1. (Color online) The red-green-blue (RGB) model on a triangular region of side length 12 ($L=4$). The three color classes of vertices are balanced along the boundary, so the boundary conditions are "flat."

relative to the global average direction, we pick an arbitrary point A, compute the winding angle from A to X, and subtract a global constant so that the average winding angle at points on the curve is 0.

When we measure the variance in the winding angle at random points along the longest loop in the RGB configuration in a region of order L, we find that the variance grows like $1\times\log L$—so in the notation of [17], $\kappa_2=1$. This wind-

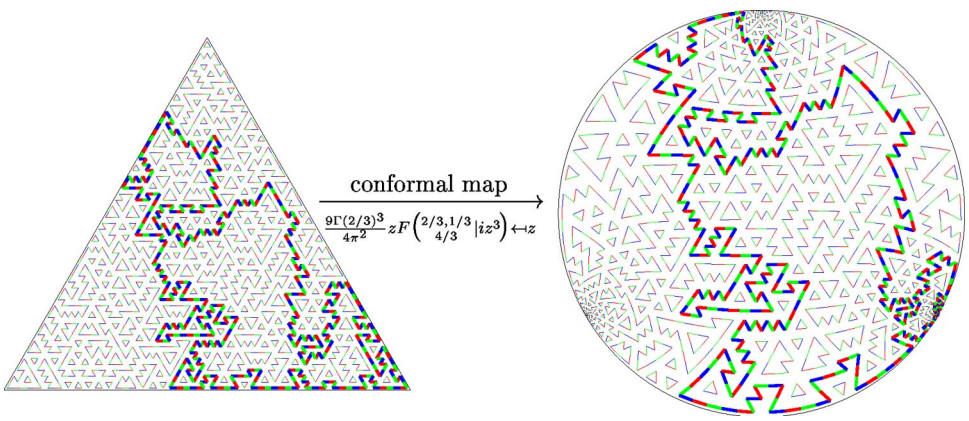

FIG. 2. (Color online) The RGB model on the triangular domain ($L=20$) is conformally mapped to a disk. The inverse conformal map, from the disk to the triangle, is the hypergeometric function shown in the diagram. If the RGB model is conformally invariant, then the loops in the disk will be rotationally invariant.

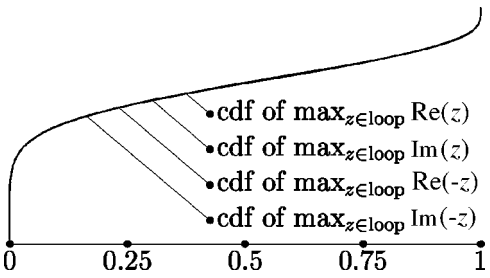

FIG. 3. In the RGB model ($L=1024$), the outermost loop surrounding the center point is selected, and conformally mapped to the disk. The image of this loop appears to be rotationally invariant; in particular, the empirical cumulative distribution functions (cdf's) for the furthest extents of the loop in the x direction, y direction, $-x$ direction, and $-y$ direction appear to coincide.

ing angle variance coefficient of 1 also shows up in the contours of FK clusters at criticality when $q=4$, and other related models such as the double-dimer model and SLE_4 (see [17–19]).

IV. CONFORMAL INVARIANCE OF RGB LOOPS

Since there is only one region, the equilateral triangle, for which we can *rapidly* generate RGB configurations, this makes the testing of conformal invariance somewhat interesting. The test that we use is similar in spirit to the tests used by Schramm to test the conformal invariance of the uniform spanning tree. We conformally mapped the RGB model on the triangular domain to a circular domain, as shown in Fig. 2. If the RGB model with flat boundary conditions were conformally invariant, then it must be that after we map a region to the disk, the resulting system of loops would be rotationally invariant. But if conformal invariance failed to hold, then there would be no particular reason to believe that the loops mapped to the disk would be rotationally invariant. After all, referring to Fig. 2, the points in the disk to which the corners of the triangle are mapped certainly look different than other points in the disk, so *a priori* we would expect the image in the disk to be anisotropic if the RGB model were not conformally invariant. As we shall see, the minimum spanning tree model fails this test, so this test is a nontrivial test of conformal invariance.

To test the rotational invariance of the image of the RGB model in the disk, we singled out the outermost loop surrounding the center of the circular domain, and collected statistics on its furthest extents in the $\pm x$ and $\pm y$ directions. If the loops in the RGB model are conformally invariant, then these four random variables would be equidistributed. But otherwise, there would be no particular reason to believe that any of these random variables (other than the first two) would have the same distributions. As shown in Fig. 3, the cumulative distribution functions for these four random variables appear to coincide, so we conclude that the RGB model appears to be conformally invariant.

V. CONFORMAL *NON*INVARIANCE OF MINIMUM SPANNING TREES

To evaluate the efficacy of our conformal invariance test, we applied it to two additional models: the minimum spanning tree and uniform spanning tree models. The minimum spanning tree (MST) is formed by assigning uniformly random edge weights to the edges of the Cartesian lattice, and picking the spanning tree (connected acyclic subset of edges) which minimizes the total weight. The uniform spanning tree (UST) is simply a spanning tree chosen uniformly at random from all spanning trees.

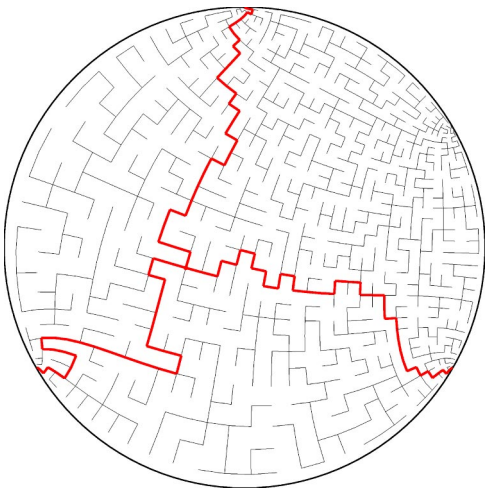

FIG. 4. (Color online) The minimum spanning tree (MST) on the 32×32 square grid, mapped conformally to the disk so that three of the corners of the square are mapped to the cube roots of unity. The paths connecting these corners are highlighted; the triple point T is the point contained in all three paths.

Figure 4 shows the MST of a square grid after it is conformally mapped to the unit disk, with three of the corners mapped to the three cube roots of unity. To test the rotational invariance of the MST after it is mapped to the disk, we looked at the paths connecting the three points at the cube roots of unity (highlighted in Fig. 4), and focused on the ''triple-point'' T contained in all three paths. If the image of MST in the disk were isotropic, then T, $e^{2\pi i/3}T$, and $e^{4\pi i/3}T$ would be equidistributed. However, as Fig. 5 illustrates, these variables are not equidistributed, so we conclude that the MST is not conformally invariant. The conformal noninvariance of the MST is surprising, given the close relationship between the MST and invasion percolation [20], the close relationship between invasion percolation and percolation, and the conformal invariance of percolation [21–23].

In contrast to the MST, the UST passes this test, as shown in Fig. 6. The triple point T connecting three boundary points of the UST is already known to be conformally invariant

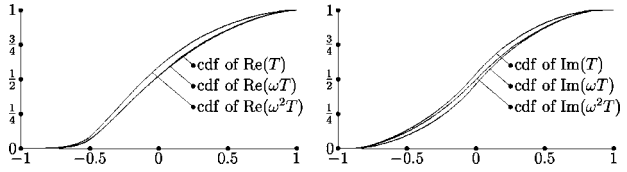

FIG. 5. The distribution of the triple point T for the MST (on the 1024×1024 grid) is not symmetric under 120° rotations, as it would be if the MST were conformally invariant. [$\omega=\exp(2\pi i/3)$.]

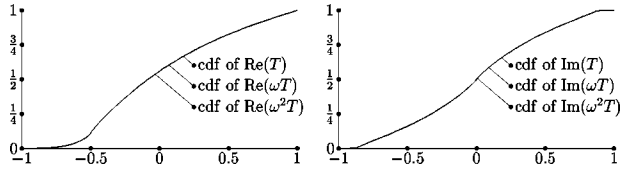

FIG. 6. In contrast, the distribution of the triple point T for the UST (on the 1024×1024 grid) passes this conformal invariance test. Kenyon [24] has proven that the triple point for UST is in fact conformally invariant (see also [25]).

[24], and indeed the entire UST process is now known to be conformally invariant [25].

Thus we learn not only that the minimum spanning tree is not conformally invariant, but that this test is a nontrivial test of conformal invariance.

VI. NESTING OF RGB LOOPS

For a scale-invariant loop model on a region of side length L, we would expect the number of loops surrounding a point to scale as $\text{const}\times\log L$. The value of this constant is a measure of how deeply nested the loops are. For the double-dimer model, Kenyon [26] proved that this nesting constant is $1/\pi^2$. (Cardy and Ziff calculate this nesting constant for FK contours [27], which is $1/\pi^2$ when $q=4$.) We measured the nesting constant of the RGB loops, and found that it is 20%–25% larger than the double-dimer nesting constant; Sheffield [28] has recently predicted this constant to be $\sqrt{3/2}/\pi^2$. Figure 7 shows that the outermost red-green-blue loops are in a sense larger than the outermost double-dimer loops, which is consistent with the red-green-blue loops being more tightly nested within one another.

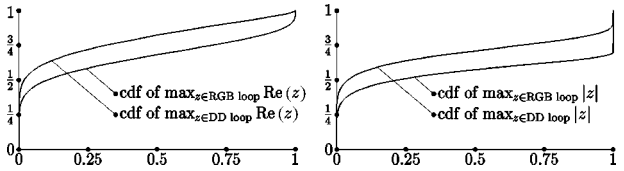

FIG. 7. Comparison of the outermost loop surrounding the origin within the red-green-blue and double-dimer models. The cdf for the size of the RGB loop is smaller than the corresponding cdf for the double-dimer loop, so in this sense the outermost RGB loop is larger than the outermost double-dimer loop. There is a good chance that the outermost RGB loop approaches the boundary quite closely, as in Fig. 2.

VII. CONCLUSIONS

Our experiments indicate that the loops of the RGB model (with flat boundary conditions) are conformally invariant and have windiness constant 1. Earlier experiments [10] have indicated that the fractal dimension is 3/2. These properties suggest that RGB loops belong to the same universality class as double-dimer loops, the fully-packed-loop model with $n=2$, and the contours of critical FK clusters with $q=4$, and are closely related to SLE_4. But the *system* of RGB loops (not just individual loops) differs from the system of double-dimer loops, as the loops are nested within one another more tightly.

ACKNOWLEDGMENT

We thank Oded Schramm for useful discussions.

[1] I. Benjamini and O. Schramm (private communication).
[2] H. Cohn, N. Elkies, and J. Propp, Duke Math. J. **85**, 117 (1996).
[3] H. Cohn, M. Larsen, and J. Propp, J. Math. Sci. (N.Y.) **4**, 137 (1998).
[4] H. Cohn, R.W. Kenyon, and J.G. Propp, J. Am. Math. Soc. **14**, 297 (2001).
[5] L.S. Levitov, Phys. Rev. Lett. **64**, 92 (1990).
[6] W. Zheng and S. Sachdev, Phys. Rev. B **40**, 2704 (1989).
[7] H.W.J. Blöte and H.J. Hilhorst, J. Phys. A **15**, L631 (1982).
[8] W. Thurston, Am. Math. Monthly **97**, 757 (1990).
[9] J. Propp, e-print math.CO/0209005.
[10] R. W. Kenyon and D. B. Wilson (unpublished).
[11] O. Schramm, Isr. J. Math. **118**, 221 (2000).
[12] C. Fortuin and P. Kasteleyn, Physica (Utrecht) **57**, 536 (1972).
[13] J. Kondev and C.L. Henley, Phys. Rev. A **74**, 4580 (1995).
[14] H.N.V. Temperley, in *London Mathematical Society Lecture Notes Series*, Vol. 13 (Mathematical Society, London, 1974), pp. 202–204.
[15] R.W. Kenyon, J.G. Propp, and D.B. Wilson, Electronic J. Comb. **7**, 591 (2000).
[16] J.G. Propp and D.B. Wilson, J. Algorithms **27**, 170 (1998).
[17] B. Wieland and D. B. Wilson (unpublished).
[18] B. Duplantier and H. Saleur, Phys. Rev. Lett. **60**, 2343 (1988).
[19] B. Duplantier and I. Binder, e-print cond-mat/0208045.
[20] J. Chayes, L. Chayes, and C.M. Newman, Commun. Math. Phys. **101**, 383 (1985).
[21] R. Langlands, P. Pouliot, and Y. Saint-Aubin, Bull. Am. Math. Soc. **30**, 1 (1994).
[22] J. Cardy, J. Phys. A **25**, L201 (1992).
[23] S. Smirnov, URL http://www.math.kth.se/~stas/papers/percol.ps.
[24] R. Kenyon, J. Math. Phys. **41**, 1338 (2000).
[25] G.F. Lawler, O. Schramm, and W. Werner, e-print math.PR/0112234.
[26] R. Kenyon, Ann. Inst. Henri Poincaré, Probab. Stat. **33**, 591 (1997).
[27] J. Cardy and R.M. Ziff, e-print cond-mat/0205404.
[28] S. Sheffield (private communication).